

THE FE LINE FLUX RATIO AS A DIAGNOSTIC OF THE MAXIMUM TEMPERATURE AND THE WHITE DWARF MASS OF CATAclySMIC VARIABLES

XIAO-JIE XU,¹ ZHUO-LI YU,¹ AND XIANG-DONG LI¹

¹*School of Astronomy and Space Science, Key Laboratory of Modern Astronomy and Astrophysics, Nanjing University, Nanjing, P. R. China 210046*

ABSTRACT

The flux ratio of Fe XXVI–Ly α to Fe XXV–He α lines ($I_{7.0}/I_{6.7}$) is a sensitive indicator of the maximum temperature (T_{\max}), and therefore the mass of white dwarf stars (M_{WD}) in cataclysmic variables (CVs). To examine and calibrate the theoretical $I_{7.0}/I_{6.7}$ – T_{\max} – M_{WD} relations, reliable measurements of T_{\max} and $I_{7.0}/I_{6.7}$ are necessary. In this work, we conduct a thorough investigation on 3–50 keV X-ray spectra of 25 solar neighborhood magnetic and non-magnetic CVs based on archival *NuSTAR* and *Suzaku* observations. The measured T_{\max} are compared to the $I_{7.0}/I_{6.7}$ and M_{WD} . The results show the sampled CVs closely follow the theoretical $I_{7.0}/I_{6.7}$ – T_{\max} relation. Moreover, all the M_{WD} estimated from $I_{7.0}/I_{6.7}$ are consistent with the dynamically measured ones. We conclude that $I_{7.0}/I_{6.7}$ can be used as a good diagnostic for T_{\max} and M_{WD} in both magnetic and non-magnetic CVs.

Keywords: binaries: close — cataclysmic variables — X-rays: binaries

1. INTRODUCTION

Cataclysmic variables (CVs) are binary stars where a white dwarf (WD) accretes matter from a main sequence/sub-giant companion via Roche-lobe overflow and/or stellar wind. CVs can be divided into magnetic ones (mCVs) and non-magnetic ones (non-mCVs) based on the magnetic field strengths of WDs (Warner 1995; Frank et al. 2002). About 20% of CVs are mCVs, including intermediate polars (IPs) and polars; the others are non-mCVs, most of which are dwarf novae (DNe) (e.g., Pretorius et al. 2013). CVs are important X-ray emitters in the luminosity range of 10^{30-34} erg s^{-1} , and were proposed to dominate the Galactic Ridge X-ray emission (e.g., Sazonov et al. 2006; Xu et al. 2016). In mCVs, more specifically IPs, matter from the companion star are channeled to magnetic poles of the WDs along the magnetic lines. A standing shock is formed near the surface of the WD, and the post-shock accreted matter is heated to tens of keV and emit X-rays. In non-magnetic CVs, on the other hand, X-rays are supposed to originate mainly from the boundary layer near the WD surface. The X-ray spectra of CVs in quiescent states can be well fitted with an isobaric absorbed cooling flow model (mkcflow in Xspec; Mushotzky & Szymkowiak 1988; Mukai et al. 2003; Suleimanov et al. 2005) with a Gaussian component to account for the fluorescent Fe $K\alpha$ line, and additional intrinsic absorption in some cases (Mukai et al. 2003). The measured maximum emission temperature (T_{\max}) of IPs are around several tens of keV, and those of non-mCVs are ~ 10 keV.

One of the fundamental questions of CVs is to measure their WD masses. The mass distribution of WDs in CVs are important for star formation and evolution theory itself. It is also closely related to other interesting astrophysical objects like progenitors of type Ia supernovae, and merging binary WDs which are supposed to be important gravitational wave emitters. Traditionally, the WD mass in a CV are derived dynamically from the radial velocity curves. This method is model-independent, but sometimes suffers from the uncertainties brought by the unknown inclination angles.

In the past two decades, X-ray spectroscopy provided an alternative method to measure the WD masses in CVs. The basic idea is that T_{\max} of a quiescent CV can be measured by fitting the X-ray continuum, and is supposed to be closely related to its WD gravitational potential, and therefore the WD mass. Assuming that the accreted matter falls from infinity (which is usually a good

approximation), T_{\max} can be estimated as M_{WD} via $T_{\max} = \frac{3}{8} \frac{\mu m_{\text{H}}}{k} \frac{GM_{\text{WD}}}{R_{\text{WD}}}$ for mCVs (where μ is the mean molecular weight, m_{H} is the mass of the H atom, k is the Boltzmann constant, G is the gravitational constant, M and R are the mass and radius of the WD, respectively. See e.g., Frank et al. 2002), and $T_{\max} = \alpha \frac{3}{16} \frac{\mu m_{\text{H}}}{k} \frac{GM}{R}$, where $\alpha = 0.65 \pm 0.07$ for non-mCVs (Yu et al. 2018). In previous works, the T_{\max} of several dozens of CVs have been measured via X-ray continuum fitting, and the derived M_{WD} were in general consistent with the dynamically determined values (e.g., Suleimanov et al. 2005; Shaw et al. 2018; Suleimanov et al. 2019).

However, reliable measurements of T_{\max} based on continuum fitting demand high S/N spectra above 10 keV, which is beyond the ability of most present-day X-ray observatories (e.g., *Chandra* and *XMM-Newton*). What's more, the T_{\max} measured this way sometimes depends on the modeling of the intrinsic absorption (e.g., pcfabs or pwab models, Ezuka & Ishida 1999; Mukai 2017), or the treatment of the reflected X-ray photons by the WD surface or the disk (e.g., Shaw et al. 2018). These issues have restricted the application of $M_{\text{WD}}-T_{\max}$ relation to limited bright CVs.

The flux ratio of Fe XXVI–Ly α (centered at ~ 7.0 keV) to Fe XXV–He α (centered at ~ 6.7 keV) emission lines ($I_{7.0}/I_{6.7}$) can be taken as a sensitive diagnostic for T_{\max} (Ezuka & Ishida 1999; Xu et al. 2016; Yu et al. 2018). The basic idea is that a higher T_{\max} ionizes more Fe atoms to hydrogen-like ions, thus leads to a higher $I_{7.0}/I_{6.7}$ (e.g., Ezuka & Ishida 1999). Comparing to the continuum fitting method, the line flux ratio method has two advantages. Firstly, most current instruments have good response in the Fe line energy so that the uncertainties of measured $I_{7.0}/I_{6.7}$ are usually small. Secondly, $I_{7.0}/I_{6.7}$ has less dependence on the continuum shape, thus could avoid the uncertainties brought by the X-ray continuum. Early works based on this method included Ezuka & Ishida (1999), who investigated a dozen of mCVs using *ASCA* observations. Recently, Xu et al. (2016) and Yu et al. (2018) measured T_{\max} and $I_{7.0}/I_{6.7}$ for a sample of *Suzaku* observed CVs, and derive the $T_{\max}-I_{7.0}/I_{6.7}-M_{\text{WD}}$ relations for Solar neighborhood non-mCVs.

However, there are still large scattering in their $T_{\max}-I_{7.0}/I_{6.7}-M_{\text{WD}}$ relations. For example, SS Cyg had a too high T_{\max} for its $I_{7.0}/I_{6.7}$. This scattering could be due to the possible systematics associated with the highly uncertain background of the Hard X-ray Detector (HXD) on board *Suzaku*,

as pointed out by [Shaw et al. \(2018\)](#). Further investigation demands higher quality X-ray spectra in 10–50 keV energy range in order to put tighter constraints on T_{\max} .

With the large effective area and the ability to focus hard X-rays up to ~ 79 keV ([Harrison et al. 2013](#)), *NuSTAR* is the most suitable instruments for this purpose. As shown in previous works, *NuSTAR* could provide high S/N spectra above 10 keV for CVs in the Solar vicinity, which were used to derive T_{\max} values (e.g., [Shaw et al. 2018](#); [Suleimanov et al. 2019](#)). Combining *NuSTAR* and *Suzaku* observations, we could reliably measure both T_{\max} and the $I_{7.0}/I_{6.7}$, and test the relations between them.

In this work, we use the *NuSTAR* and *Suzaku* observations on CVs in the Solar vicinity to make updated $I_{7.0}/I_{6.7}-T_{\max}-M_{\text{WD}}$ relations for both IPs and non-mCVs. We describe our data and method in Section 2. We present the results and examine the relations in Section 3, we make brief discussion in Section 4 and summarize in section 5. Throughout this work, we quote errors at 90% confidence level, unless otherwise stated.

2. DATA & ANALYSIS

We choose *NuSTAR* and *Suzaku* as the main instruments in this work. *NuSTAR* contains two focal plane modules, FPMA and FPMB, and is capable to focus X-rays up to ~ 79 keV ([Harrison et al. 2013](#)), which is suitable to measure T_{\max} of CVs. The *Suzaku* X-ray Observatory operated between 2005 and 2015. It had two types of instruments: the X-ray Imaging Spectrometers (XIS, [Koyama et al. 2007](#)), and the HXD ([Takahashi et al. 2007](#)). The XIS consists of four sensors: one is made of back-illuminated CCD (XIS-1), and the other three are made of front-illuminated CCDs (XIS-0, 2, 3). XIS-2 suffered catastrophic damage on 2006 November 9 and no useful data have been transferred since then. The XIS detectors had the spectral resolution of ~ 20 –50 among the Fe line energy range and are suitable for $I_{7.0}/I_{6.7}$ measurements.

We select a sample of CVs in the Solar vicinity based on archival *NuSTAR* and *Suzaku* observations. Firstly, we carefully select CVs in quiescent states from the *Suzaku* samples of [Xu et al. \(2016\)](#) and [Yu et al. \(2018\)](#) to maximize counting statistics in the Fe line range. The selection results in a sample of 25 CVs, 13 of which (including 5 IPs and 8 non-mCVs) have dynamical mass measurements and 12

(including 11 IPs and 1 non-mCVs) without mass measurements. The observation log of the sampled CVs are listed in Table 1. We further cross-correlate this CV sample with *NuSTAR* archive, and find observations on 12 IPs and 2 non-mCVs. The observation log of this sub-sample are also presented in Table 1. Seven of the fourteen *NuSTAR* observations on sampled CVs have been previously analyzed, including EX Hya, FO Aqr, RX J2133+5107, NY Lup, TV Col, V1223 Sgr and V709 Cas (Shaw et al. 2018; Suleimanov et al. 2019). The other seven observations are first analyzed in this work, including BG CMi, XY Ari, AO Psc, IGR J1719-4100, V2400 Oph, BZ UMa and SS Cyg.

We reduce the *NuSTAR* data using the NuSTAR Data Analysis Software (NSuTARDAS v1.9.3), packaged with HEASOFT v6.25 and the latest CALDB (version 20190314) files. The data reduction is performed using the standard pipeline (nupipeline command in heasoft) and the cleaned event files are produced. We further use nuproducts command to generate spectra, the rmf and arf files. For each source, a $100''$ circular region centered on the source is used to extract the source spectra, and a co-centered annulus with inner and outer radii of $130''$ and $200''$ to extract the background spectra. We also vary the radii of the source regions to $70''$ or $130''$, and the the background region to circular regions in the same CCD with the sources, and find that the results are not sensitive to these variations. We then conclude that the spectra extraction procedures are robust. We groupe all spectra using grppha so that the signal-to-noise ratio of each bin exceeds three.

We reduce the *Suzaku* data with the standard pipeline *aepipeline* with the latest calibration files (XIS: 20181010, HXD: 20110913 and XRT: 20110630). For each XIS screening image, we use xselect tools to extract the source events from a $200''$ circular region ($120''$ circular region if the source is too close to the CCD edges) and background events from a $250'' - 400''$ annulus, excluding regions outside CCD or contaminating sources. The results are not sensitive to the exact selection of the background, because the sources are all quite bright. For HXD data, the background files are downloaded from Suzaku background FTP server and the spectra are generated with the *hxdpinxbpi* tool. All XIS and HXD spectra are regrouped so that the signal-to-noise ratio of each bin exceeded three.

Following Yu et al. (2018) and Shaw et al. (2018), the T_{\max} of individual CVs with available *NuSTAR* observations is measured by fitting the 3–50 keV *NuSTAR* spectra with an absorbed mkcflow

Table 1. Observation log and dynamically measured WD masses of CVs. Sources in bold fonts were observed by both *NuSTAR* and *Suzaku*, others were only observed by *Suzaku*.

Source	<i>NuSTAR</i> Obs-ID	<i>Suzaku</i> Obs-ID	M_{WD} (M_{\odot})
IPs			
BG CMi	30460018002	404029010	0.8 ± 0.2^a
EX Hya	30201016002	402001010	$0.5 \pm 0.05^b / 0.79 \pm 0.026^c$
TV Col	30001020002	403023010	0.75 ± 0.15^d
XY Ari	30460006002	500015010	1.04 ± 0.13^e
YY Dra	—	403022010	0.83 ± 0.1^f
AO Psc	30460008002	404033010	—
FO Aqr	30460002002	404032010	—
IGR J1719–4100	30460005002	403028010	—
RX J2133.7+5107	30460001002	401038010	—
MU CaM	1.03 ± 0.18	403004010	—
NY Lup	30001146002	401037010	—
PQ Gem	—	404030010	—
TX Col	—	404031010	—
V709 Cas	30001145002	403025010	—
V1223 Sgr	30001144002	408019020	—
V2400 Oph	30460003002	403021010	—
Non-mCVs			
V893 Sco	—	401041010	0.89 ± 0.15^g
SS Aur	—	402045010	1.08 ± 0.4^h
BZ UMa	30201019002	402046010	$0.65^{+0.50}_-0.21^i$
VW Hyi	—	406009030	0.67 ± 0.22^j
U Gem	—	407034010	1.2 ± 0.05^k
EK Tra	—	407044010	0.46 ± 0.10^l
BV Cen	—	407047010	$0.83 \pm 0.1^m / 1.24 \pm 0.22^n$
SS Cyg	80202036002	400006010	1.1 ± 0.2^o
V1159 Ori	—	408029010	—

The reference for the dynamically determined M_{WD} : a: Penning (1985), b: Beuermann et al. (2003), c: Beuermann & Reinsch (2008), d: Hellier (1993), e: Hellier (1997), f: Haswell et al. (1997), g: Mason et al. (2001), a $0.15M_{\odot}$ uncertainty is assumed h: Sion et al. (2008), i: Jurcevic et al. (1994), j: Hamilton et al. (2011), k: Ritter & Kolb (2003), l: Gansicke et al. (1997), m: Gilliland (1982), n: Watson et al. (2007), o: Friend et al. (1990)

model, $\text{pha} \times (\text{mkcflow} + \text{Gaussian})$, or $\text{pha} \times \text{pcfabs} \times (\text{mkcflow} + \text{Gaussian})$ if additional absorption is needed. The *mkcflow* model describes the X-ray emission, and the Gaussian represents the fluorescent Fe $K\alpha$ lines centering around 6.4 keV, respectively. The *pha* and *pcfabs* components describe the foreground and intrinsic absorption of the CV, respectively. The values of T_{max} would vary up to $\sim 5\%$ if the IPM model¹ was adopted, hence we conclude that the *mkcflow* model is robust. For CVs without *NuSTAR* observations, their T_{max} are measured by fitting the 3–50 keV *Suzaku* spectra with the same model as for the *NuSTAR* spectra.

The $I_{7.0}/I_{6.7}$ values of individual CVs are adopted from Xu et al. (2016) except XY Ari. The $I_{7.0}/I_{6.7}$ of XY Ari is re-measured to be 0.94 ± 0.2 , which is consistent with the recent XMM-Newton observations (Zengin Camurdan et al. 2018), and is higher than the value (0.62 ± 0.10) obtained by Xu et al. (2016).

The theoretical $I_{7.0}/I_{6.7}-T_{\text{max}}-M_{\text{WD}}$ relations are derived separately for IPs and non-mCVs, following Xu et al. (2016) and Yu et al. (2018). Briefly, we generate a series of simulated spectra, by using the *mkcflow* model and assigning different T_{max} (hence M_{WD}) values. The simulated spectra are then fitted, the corresponding $I_{7.0}/I_{6.7}$ measured, in the exact same way as for the real spectra analyzed above.

3. RESULTS

Tables 2 summarize the fitting results of individual CVs, also listed are the WD masses measured dynamically (if available) and those derived from $I_{7.0}/I_{6.7}$ and T_{max} . In general, the model fitting is acceptable, judged by the χ^2_{ν} values. We present in Figure 1 the 3–50 keV *NuSTAR* spectra, together with the best-fitted models, for two CVs (BG CMi and SS Cyg) as an example.

Figure 2 and Figure 3 show $I_{7.0}/I_{6.7}$ versus T_{max} , and $I_{7.0}/I_{6.7}$ versus dynamical M_{WD} of the sampled sources, respectively. EX Hya and BV Cen are not included in Figure 3 due to multiple dynamical M_{WD} values. The $I_{7.0}/I_{6.7}-T_{\text{max}}$ and $I_{7.0}/I_{6.7}-M_{\text{WD}}$ relations predicted by the *mkcflow* model are

¹ The IPM model is not used in this work because it does not contain description of Fe lines. Also see Shaw et al. (2018) for a comparison of the *mkcflow* and IPM models.

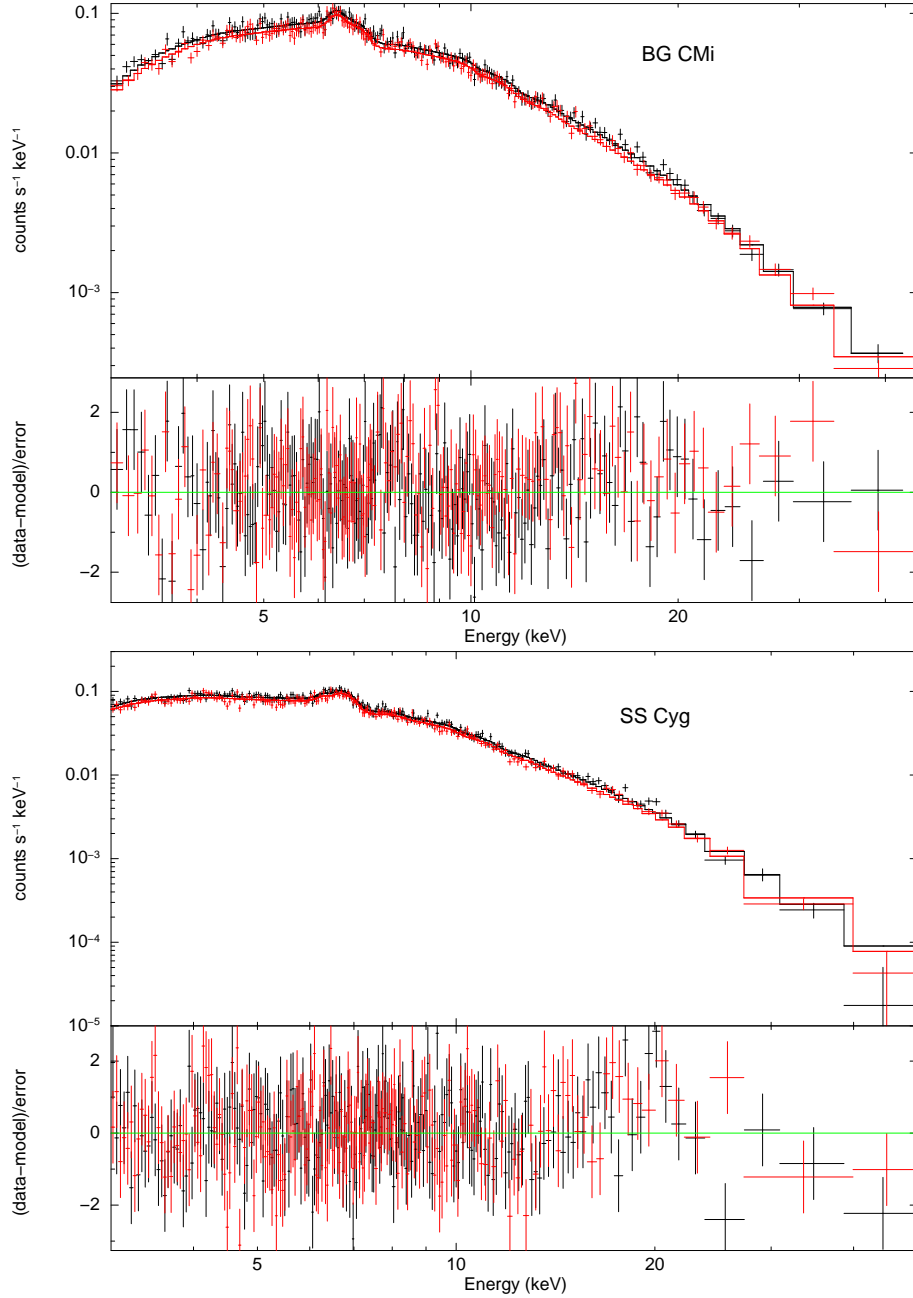


Figure 1. Examples of typical 3–50 keV *NuSTAR* spectra of two CVs, with the best-fitted model of an absorbed mckflow plus a Gaussian to model the Fe $K\alpha$ line. The black and red data points represent FPMA and FPMB spectra, respectively. The upper and lower panels are spectra of BG CMi and SS Cyg, respectively. Spectra are rebinned for plotting only.

plotted as solid and dashed curves in both figures, which are to be contrasted with sampled CVs. We present the predicted relations for 0.1 and 1 solar abundances in both figures to cover different populations of CVs following Yu et al. (2018), e.g., those in the Solar neighborhood/Galactic bulge

Table 2. Observed and derived properties of CVs. Sources in bold fonts were observed by both *NuSTAR* and *Suzaku*, others were observed by *Suzaku* only. T_{\max} from previous works are also listed for comparison.

Source	N_{H} 10^{22} cm^{-2}	$N_{\text{H,pc}}$ 10^{22} cm^{-2}	C.F.	$I_{7.0/6.7}$	T_{\max}^a (keV)	$\chi^2_{\nu}/\text{d.o.f.}$	T_{\max}^b (keV)	M_{WD}^c (M_{\odot})	M_{WD}^d (M_{\odot})	M_{WD}^e (M_{\odot})
IPs										
BG CMi	6.6 ± 1.8	61 ± 25	0.37 ± 0.07	0.71 ± 0.18	32.5 ± 6.0	0.98/687	24.1 ± 4.6^{b1}	0.75 ± 0.12	0.75 ± 0.07	0.8 ± 0.2
EX Hya*	< 1.1	16_{-7}^{+16}	$0.25_{-0.13}^{+0.06}$	0.39 ± 0.02	14.5 ± 0.3	1.10/603	16.7 ± 2.3^{b1}	0.77 ± 0.10	0.76 ± 0.07	$0.5 \pm 0.05/0.79 \pm 0.026$
TV Col	$3.1_{-1.2}^{+0.90}$	49 ± 17	0.30 ± 0.05	0.67 ± 0.08	30.1 ± 2.1	1.01/863	36.0 ± 3.5^{b1}	0.72 ± 0.06	0.73 ± 0.02	0.75 ± 0.15
XY Ari	1.7 ± 1.3	–	–	0.94 ± 0.2	57.5 ± 7.9	1.03/76	$67.0_{-14.8}^{+19.5 b1}$	0.91 ± 0.27	0.99 ± 0.06	1.04 ± 0.13
YY Dra	< 0.66	$76+30_{-14}$	0.33 ± 0.13	0.80 ± 0.16	37.8 ± 4.0	1.01/4516	33.1 ± 7.6^{b1}	0.80 ± 0.14	0.82 ± 0.04	0.83 ± 0.1
AO Psc	2.6 ± 1.1	41 ± 9.0	0.47 ± 0.06	0.56 ± 0.06	17.9 ± 1.2	1.10/770	17.5 ± 3.4^{b1}	0.58 ± 0.04	0.53 ± 0.03	–
FO Aqr	3.8 ± 2.3	33 ± 5.5	0.70 ± 0.07	0.58 ± 0.12	22.3 ± 1.5	1.11/662	20.8 ± 1.4^{b1}	0.61 ± 0.11	0.61 ± 0.03	–
J1719–4100	2.1 ± 1.0	74 ± 46	0.22 ± 0.06	0.87 ± 0.20	37.8 ± 4.8	1.08/675	30.2 ± 5.3^{b1}	$0.85_{-0.15}^{+0.29}$	0.82 ± 0.04	–
J2133.7+5107	3.6 ± 0.79	142 ± 23	0.59 ± 0.04	0.88 ± 0.11	47.3 ± 7.5	1.07/581	52.0 ± 5.5^{b1}	0.87 ± 0.10	0.91 ± 0.07	–
MU Cam	3.81 ± 1.15	63 ± 20	0.56 ± 0.08	1.03 ± 0.18	41.9 ± 11.6	0.95/2874	26.7 ± 5.8^{b1}	$1.17_{-0.33}^{+0.08}$	0.86 ± 0.10	–
NY Lup	4.1 ± 0.55	205 ± 26	0.49 ± 0.03	1.03 ± 0.16	53.2 ± 5.1	0.94/592	$55.5_{-3.4}^{+6.9 b2}$	$1.17_{-0.30}^{+0.07}$	0.94 ± 0.04	–
PQ Gem	< 2.93	40 ± 24	0.37 ± 0.12	0.77 ± 0.26	40.5 ± 3.8	0.94/4589	34.6 ± 5.7^{b1}	$0.78_{-0.23}^{+0.28}$	0.84 ± 0.04	–
TX Col	2.5 ± 0.81	73 ± 20	0.56 ± 0.10	0.63 ± 0.14	22.4 ± 3.5	0.90/3648	17.7 ± 3.4^{b1}	0.67 ± 0.11	0.60 ± 0.05	–
V709 Cas	107 ± 48	–	–	0.97 ± 0.20	43.5 ± 6.8	1.05/598	$50.0_{-3.9}^{+4.6 b2}$	$0.94_{-0.28}^{+0.16}$	0.88 ± 0.05	–
V1223 Sgr	3.0 ± 0.7	66 ± 10	0.46 ± 0.03	0.8 ± 0.08	32.4 ± 2.5	1.11/803	$35.4_{-1.5}^{+1.7 b2}$	0.81 ± 0.06	0.75 ± 0.03	–
V2400 Oph	2.8 ± 0.6	111 ± 16	0.48 ± 0.04	0.73 ± 0.05	30.9 ± 2	1.03/636	30.2 ± 3.9^{b1}	0.75 ± 0.04	0.74 ± 0.04	–
Non-mCVs										
V893 Sco	1.96 ± 0.44	–	–	0.37 ± 0.07	15.7 ± 1.1	0.91/2767	–	0.84 ± 0.08	0.92 ± 0.03	0.89 ± 0.15
SS Aur	< 2.08	–	–	0.56 ± 0.2	26.3 ± 2.9	0.91/919	–	1.03 ± 0.07	1.13 ± 0.05	1.08 ± 0.4
BZ UMa	< 0.9	32 ± 25	0.36 ± 0.21	0.4 ± 0.16	13.6 ± 0.4	1.2/102	13.6 ± 0.9^{b3}	0.87 ± 0.15	0.85 ± 0.03	$0.65_{-0.21}^{+0.50}$
VW Hyi	< 1.14	–	–	0.21 ± 0.07	9.7 ± 0.5	0.98/1441	–	0.63 ± 0.11	0.73 ± 0.03	0.67 ± 0.22
U Gem	< 0.86	–	–	0.68 ± 0.08	26.9 ± 0.6	1.07/3387	–	1.18 ± 0.03	1.14 ± 0.01	1.2 ± 0.05
EK Tra	< 0.54	–	–	0.16 ± 0.08	10.4 ± 0.5	1.07/2425	–	0.60 ± 0.10	0.75 ± 0.02	0.46 ± 0.10
BV Cen	< 0.86	–	–	0.51 ± 0.09	25.1 ± 2.2	1.04/2866	–	1.02 ± 0.20	1.12 ± 0.03	$0.83 \pm 0.1/1.24 \pm 0.22$
SS Cyg	< 0.86	60 ± 11	0.3 ± 0.07	0.73 ± 0.07	26.9 ± 1.4	1.03/665	42.1 ± 1.0^{b3}	1.20 ± 0.03	1.07 ± 0.02	1.1 ± 0.2
V1159 Ori	< 1.05	–	–	0.16 ± 0.14	9.29 ± 0.60	1.01/1855	–	0.60 ± 0.15	0.70 ± 0.03	–

N_{H} and $N_{\text{H,pc}}$ represent foreground and partial covering absorption column density, respectively. C.F. is the covering fraction.

a: T_{\max} from this work. b: T_{\max} from previous works, including b1: T_{\max} derived from the M_{WD} values from [Suleimanov et al. \(2019\)](#), assuming the accreted matter falls from infinity; b2: T_{\max} from [Shaw et al. \(2018\)](#); b3: T_{\max} from [Yu et al. \(2018\)](#). c: M_{WD} derived from $I_{7.0}/I_{6.7}$ of this work. d: M_{WD} derived from T_{\max} of this work. e: Dynamically measured M_{WD} . *: The magnetospheric radius is taken into consideration when deriving M_{WD} of EX Hya from its $I_{7.0}/I_{6.7}$ and T_{\max} values ([Suleimanov et al. 2019](#)).

and near the Galactic center, respectively. It can be seen that the individual CVs generally follows the predicted $I_{7.0}/I_{6.7}-T_{\max}$ and $I_{7.0}/I_{6.7}-M_{\text{WD}}$ relations in wide ranges (0.2–1.0 for $I_{7.0}/I_{6.7}$ and 10–60 keV for T_{\max} , respectively), especially those of a sub-solar metallicity ($Z = 0.1$). This might reflect the relatively low metallicity of the sample CVs (with a mean $Z \sim 0.3$, see [Nobukawa et al. 2016](#)). We then conclude that $I_{7.0}/I_{6.7}$ is a good indicator of T_{\max} .

4. DISCUSSION

4.1. Comparison to Previous Studies & Limitations

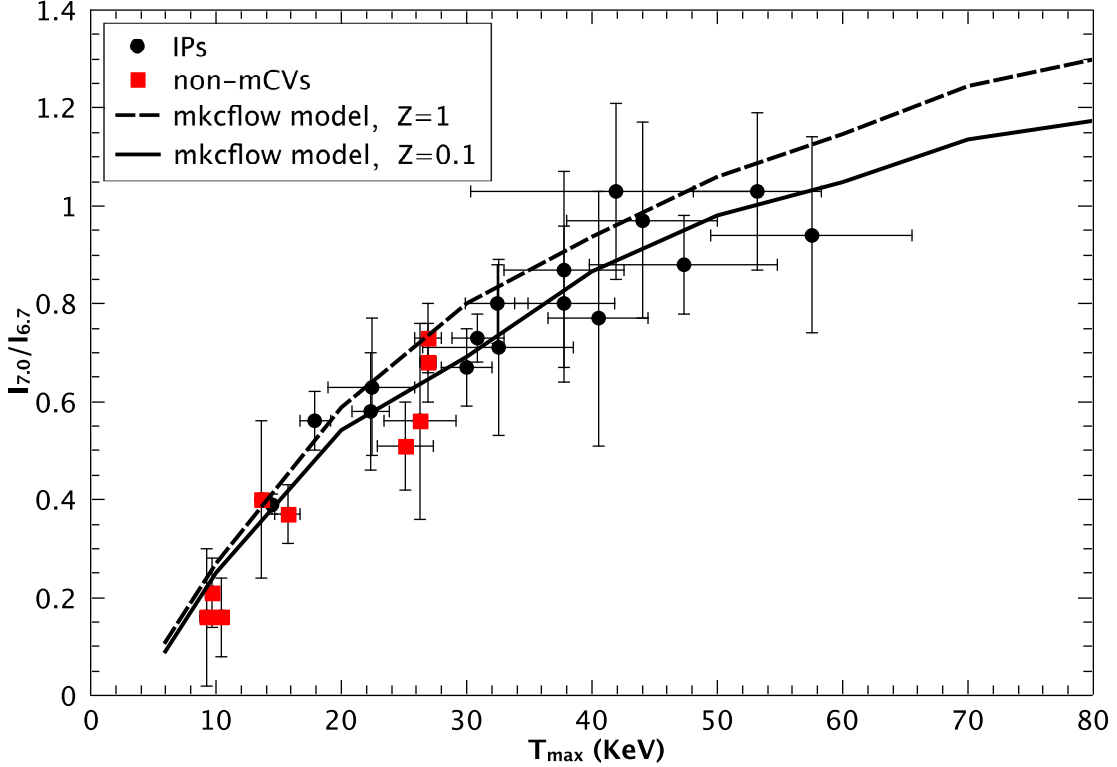


Figure 2. $I_{7.0}/I_{6.7}$ versus T_{\max} for sampled CVs. Symbols and lines are as described in the insert. The solid and dashed black curves are the predicted relations by mkcflow models of different metallicities ($Z = 0.1$ and 1 solar values, respectively).

Various studies on Solar neighborhood CVs have been carried out previously using different instruments. For example, Yu et al. (2018), Shaw et al. (2018) and Suleimanov et al. (2019) have utilized *Suzaku*, *NuSTAR* and *Swift*/BAT observations of CVs to measure their T_{\max} values. It would be helpful to compare our results with theirs. From Table 2, the T_{\max} in this work are in general consistent with previous measurements (Suleimanov et al. 2005, 2019; Shaw et al. 2018; Yu et al. 2018). The only exception is SS Cyg. From the new *NuSTAR* data, the T_{\max} of SS Cyg is measured to be 26.9 ± 1.4 keV, which is significantly lower than previous values (42.1 ± 1.0 keV by Yu et al. 2018, $52.5^{+1.1}_{-0.7}$ by Wada et al. 2017, or $41.99^{+1.20}_{-0.76}$ keV by Byckling et al. 2010). We speculate that the differences are resulting from the uncertain background of *Suzaku* HXD which was used in these previous works, as suggested by Shaw et al. (2018). Actually, unlike the old values, the new T_{\max} of SS Cyg closely follow the $I_{7.0}/I_{6.7}-T_{\max}$ relation (see Figure 2, also see Figure 2 of Yu et al. 2018).

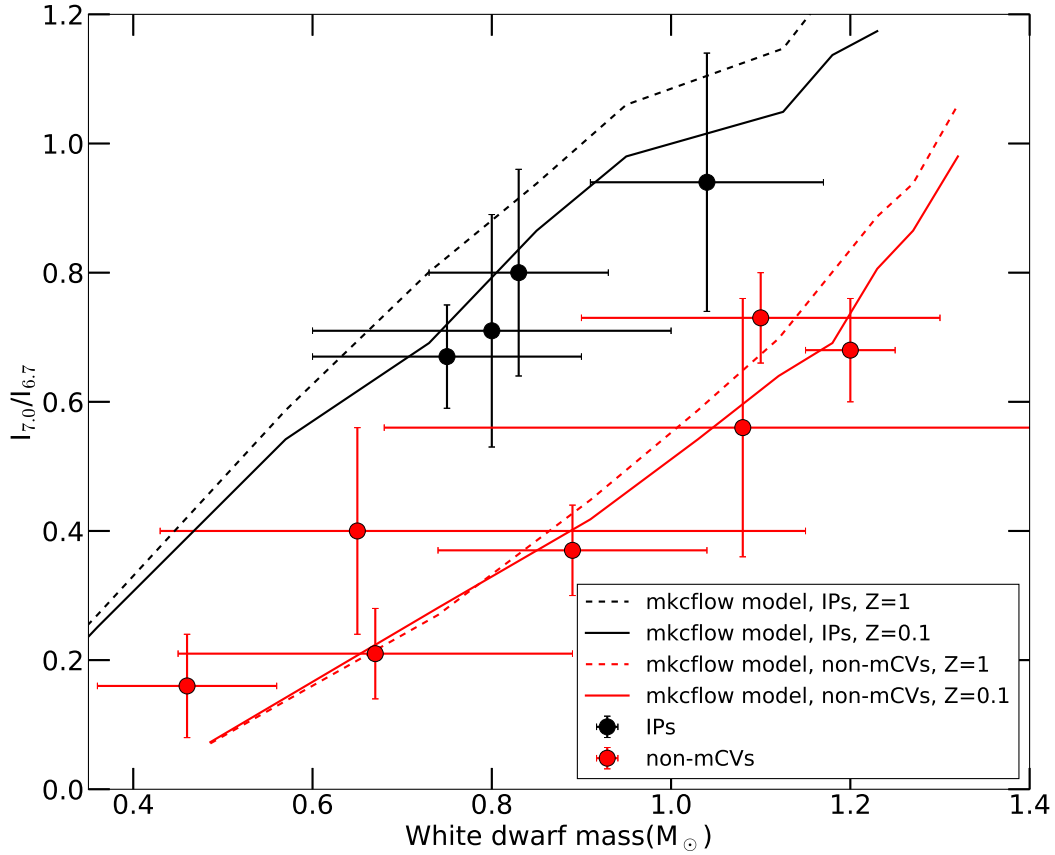


Figure 3. $I_{7.0}/I_{6.7}$ vs. dynamical M_{WD} for sampled CVs. The black (red) solid and dashed curves are the predicted relations by mkcflow for IPs (non-mCVs) with abundances set to 0.1 and 1 solar values, respectively.

This consistency further shows the advantage of $I_{7.0}/I_{6.7}$ to derive T_{max} comparing to the continuum fitting method.

The limitations in this work are addressed as follows. Firstly, the reflection component and the magnetospheric radius of WDs were not considered when fitting the continuum in this work, which may add uncertainties to measured T_{max} values, as discussed by [Suleimanov et al. \(2019\)](#); [Shaw et al. \(2018\)](#). The modeling of the intrinsic absorption of IPs may also affect the measured T_{max} (e.g., [Mukai et al. 2003](#); [Mukai 2017](#)). All these factors may add complication to measured T_{max} . Further investigations on these issues are necessary to improve the $T_{\text{max}}-I_{7.0}/I_{6.7}-M_{\text{WD}}$ relations.

Secondly, the sample size is still small. As the currently best available CV sample, our sample only includes 25 CVs (only 11 of which have dynamical M_{WD} measurements), which is obviously statistically incomplete, and might be biased to relatively bright sources. Moreover, our sample are lack of WDs more massive than $1.2M_{\odot}$, which could restrict the application of the relations to less massive WDs. The derived $T_{\text{max}}-I_{7.0}/I_{6.7}-M_{\text{WD}}$ relations should be checked against less luminous CVs, and CVs with more massive WDs in the future.

Thirdly, the dynamical mass uncertainties are large. EX Hya and BV Cen have multiple, inconsistent dynamical mass measurements so that they have to be excluded from the analysis. For the other 11 CVs presented in Figure 4, the typical error range of optically determined M_{WD} is $\sim 0.1 - 0.2M_{\odot}$ (see Table 1), which is already comparable, if not greater than those of M_{WD} derived from $I_{7.0}/I_{6.7}$ and T_{max} ($\sim 0.05 - 0.1M_{\odot}$, see Table 2). As a result, the uncertainties in the $I_{7.0}/I_{6.7}-M_{\text{WD}}$ and $I_{7.0}/I_{6.7}-T_{\text{max}}$ relations are dominated by the dynamically measured M_{WD} values. What's more, careful calibrations on the dynamical WD masses in CVs may be necessary, because the presence of the 'hot spot' or the non-circular motions in the outer accretion disk could distort the radial velocity curves of the optical emission and absorption lines (Marsh et al. 1987; Hessman et al. 1989). More reliable WD masses measurements are needed to improve the $I_{7.0}/I_{6.7}-M_{\text{WD}}$ relations.

4.2. $I_{7.0}/I_{6.7}$ as a Diagnostic of T_{max} and M_{WD} of CVs

Judged from Table 1 and Table 2, $I_{7.0}/I_{6.7}$ is a good indicator of T_{max} , however, is it also a good diagnostic for M_{WD} ? To address this issue, we compare the M_{WD} derived from $I_{7.0}/I_{6.7}$ (assuming 0.1 solar abundance) and T_{max} to the dynamically measured values for both IPs and non-mCVs in Figure 4. It is obvious that all M_{WD} derived from $I_{7.0}/I_{6.7}$ are consistent with the dynamical measured values. On the other hand, although M_{WD} derived from T_{max} in general show smaller uncertainties, there is one CV, EK TrA, whose derived M_{WD} is not consistent with the dynamical value.

To quantify the goodness of the derived M_{WD} , we assume the the following linear relation $M_{\text{WD,derived}} = A \times M_{\text{WD,dynamical}} + B$ and perform fitting for derived M_{WD} . The best-fit yields $A = 0.97 \pm 0.09$ and $B = 0.06 \pm 0.09$, with $\chi_{\nu}^2 = 1.6$ and $r^2 = 0.94$ for $I_{7.0}/I_{6.7}$ derived M_{WD} , and $A = 0.62 \pm 0.02$ and $B = 0.38 \pm 0.03$, with $\chi_{\nu}^2 = 8.0$ and $r^2 = 0.91$ for T_{max} derived M_{WD} . Judged from

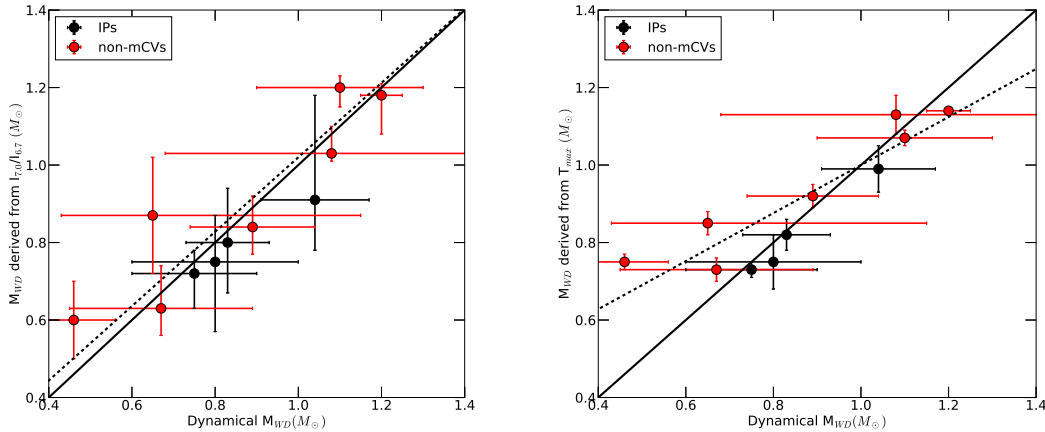


Figure 4. Left panel: M_{WD} derived from $I_{7.0}/I_{6.7}$ versus dynamically determined M_{WD} . Right panel: M_{WD} derived from T_{max} versus dynamically determined M_{WD} . The black (red) data points represent IPs (non-mCVs). The solid diagonal lines in both panels show a 1:1 relation for the M_{WD} values. The dashed lines show the best linear fit to the distribution (see Section 4.2 for details).

the fitting results, $I_{7.0}/I_{6.7}$ derived M_{WD} are more consistent with the optical ones. This comparison do not necessarily imply that $I_{7.0}/I_{6.7}$ is intrinsically a better indicator of M_{WD} compared to T_{max} , since the latter may be biased due to data quality and continuum modeling. Nevertheless, based on the current data, this comparison suggests that $I_{7.0}/I_{6.7}$ is an as good diagnostic of the M_{WD} of both IPs and non-mCVs compared to T_{max} .

5. SUMMARY

We have systematically analyzed *NuSTAR* and *Suzaku* observations on a sample of 25 solar neighborhood CVs, including 16 IPs and 9 non-mCVs to investigate their $T_{\text{max}}-I_{7.0}/I_{6.7}-M_{\text{WD}}$ relations. Our main results can be summarized as follows:

- a) The measured T_{max} are in general consistent with previous results except SS Cyg, which shows a lower temperature (26.9 ± 1.4 keV) comparing to previous results ($\sim 40-50$ keV).
- b) $I_{7.0}/I_{6.7}$ of both IPs and non-mCVs follow the theoretical $I_{7.0}/I_{6.7}-T_{\text{max}}$ relation, which covers a wide $I_{7.0}/I_{6.7}$ range of $\sim 0.1-1.0$, and a wide T_{max} range of $\sim 10-60$ keV.
- c) The M_{WD} derived from $I_{7.0}/I_{6.7}$ are more consistent with the dynamically measured values com-

pared to those derived from T_{\max} , showing that $I_{7.0}/I_{6.7}$ is a good diagnostic of M_{WD} in CVs.

The authors thank the anonymous referee for constructive comments that helped improve this paper. This work is supported by the Natural Science Foundation of China under grant Nos. 11873029, 11333004, and 11773015, Project U1838201 supported by NSFC and CAS, and the National Key Research and Development Program of China (2016YFA0400803). This work made use of data from the *NuSTAR* mission, a project led by the California Institute of Technology, managed by the Jet Propulsion Laboratory, and funded by the National Aeronautics and Space Administration. We thank the *NuSTAR* Operations, Software and Calibration teams for support with the execution and analysis of these observations. This research has made use of the *NuSTAR* Data Analysis Software (NuSTARDAS) jointly developed by the ASI Science Data Center (ASDC, Italy) and the California Institute of Technology (USA).

REFERENCES

- Beuermann, K., Harrison, Th. E., McArthur, B. E., Benedict, G. F., & Gansicke, B. T., 2003, *A&A*, 412, 821
- Beuermann, K., & Reinsch, K. 2008, *A&A*, 480, 199B
- Byckling K., Mukai K., Thorstensen J. R., & Osborne J. P., 2010, *MNRAS*, 408, 2298
- Ezuka, H., & Ishida, M., 1999, *ApJS*, 120, 277
- Frank, J., King, A., & Raine, D. 2002, *Accretion Power in Astrophysics* (Cambridge: Cambridge Univ. Press)
- Friend, M. T., Martin, J. S., Connon-Smith, R., & Jones, D. H. P. 1990, *MNRAS*, 246, 654
- Gansicke, B. T., Beuermann, K., & Thomas, H. C. 1997, *MNRAS*, 289, 388
- Gilliland, R. L., 1982, *ApJ*, 263, 302
- Hamilton, R. T., Harrison, T. E., Tappert, C., & Howell, S. B. 2011, *ApJ*, 728, 16
- Harrison F. A., Craig, W. W., Christensen, F. E. et al., 2013, *ApJ*, 770, 103
- Haswell, C. A., Patterson, J., Thorstensen, J. R., Hellier, C., & Skillman, D. R., 1997, *ApJ*, 476, 847H
- Hellier, C., 1993, *MNRAS*, 264, 132H
- Hellier, C., 1997, *MNRAS*, 291, 71
- Hessman, F. V., Koester, D., Schoembs, R., & Barwig, H., 1989, *A&A*, 213, 167

- Jurcevic, J. S., Honeycutt, R. K., Schlegel, E. M., & Webbink, R. F. 1994, *PASP*, 106, 481
- Koyama, K., Tsunemi, H., Dotani, T., et al. 2007, *PASJ*, 59, 23
- Marsh, T. R., Horne, K., & Shipman, H. L., *MNRAS*, 225, 551
- Mason, E., Skidmore, W., Howell, S. B., & Mennickent, R. E. 2001, *ApJ*, 563, 351
- Mukai, K., Kinkhabwala, A., Peterson, J. R., Kahn, S. M., & Paerels, F. 2003, *ApJ*, 586, L77
- Mukai, K. 2017, *PASP*, 129, 2001
- Mushotzky, R. F., & Szymkowiak, A. E. 1988, in *NATO ASIC Proc. 229: Cooling Flows in Clusters and Galaxies*, ed. A. C. Fabian (Dordrecht: Kluwer Academic Publishers), 53
- Nobukawa, M., Uchiyama, H., Nobukawa, K. K., Yamauchi, S., & Koyama, K. 2016, *ApJ*, 833, 268
- Penning, W. R., 1985, *ApJ*, 289, 300P
- Pretorius, M. L., Knigge, C., & Schwope, A. D. 2013, *MNRAS*, 432, 570
- Ritter, H., & Kolb, U. 2003, *A&A*, 404, 301
- Sazonov, S., Revnivtsev, M., Gilfanov, M., et al. 2006, *A&A*, 450, 117
- Shaw, A. W., Heinke, C. O., Mukai, K. et al., 2018, *MNRAS*, 476, 554
- Sion, E. M., Gnsicke, B. T., Long, K. S., et al. 2008, *ApJ*, 681, 543
- Suleimanov, V., Revnivtsev, M., & Ritter, H. 2005, *A&A*, 435, 191
- Suleimanov, V. F., Doroshenko, V., Werner, K., 2019, *MNRAS*, 482, 3622
- Takahashi, T., Abe, K., Endo, M., et al. 2007, *PASJ*, 59, 35
- Wada, Q., Tsujimoto, M., Ebisawa, K., & Hayashi, T. 2017, *PASJ*, 69, 10
- Warner, B. 1995, *Cataclysmic Variable Stars* (Cambridge: Cambridge Univ.Press)
- Watson, C. A., Steeghs, D., Shahbaz, T., & Dhillon, V. S., 2007, *MNRAS*, 382, 1105
- Xu, X.-j., Wang, Q. D., & Li, X.-D. 2016, *ApJ*, 818, 136
- Yu, Z., Xu, X.-j., Li, X.-D et al., 2018, *ApJ*, 853, 182
- Yuasa, T., Nakazawa, K., Makishima, K., et al. 2010, *A&A*, 520, 25
- Zengin Camurdan, D., Balman, S., & Burwitz, V., 2018, *MNRAS*, 477, 4035